SCIENTIFIC REP⚙RTS

OPEN

Calculation of exchange integrals and Curie temperature for La-substituted barium hexaferrites

Chuanjian Wu[1], Zhong Yu[1], Ke Sun[1], Jinlan Nie[2], Rongdi Guo[1], Hai Liu[1], Xiaona Jiang[1] & Zhongwen Lan[1]

As the macro behavior of the strength of exchange interaction, state of the art of Curie temperature T_c, which is directly proportional to the exchange integrals, makes sense to the high-frequency and high-reliability microwave devices. Challenge remains as finding a quantitative way to reveal the relationship between the Curie temperature and the exchange integrals for doped barium hexaferrites. Here in this report, for La-substituted barium hexaferrites, the electronic structure has been determined by the density functional theory (DFT) and generalized gradient approximation (GGA). By means of the comparison between the ground and relative state, thirteen exchange integrals have been calculated as a function of the effective value U_{eff}. Furthermore, based on the Heisenberg model, the molecular field approximation (MFA) and random phase approximation (RPA), which provide an upper and lower bound of the Curie temperature T_c, have been adopted to deduce the Curie temperature T_c. In addition, the Curie temperature T_c derived from the MFA are coincided well with the experimental data. Finally, the strength of superexchange interaction mainly depends on $2b$-$4f_1$, $4f_2$-$12k$, $2a$-$4f_1$, and $4f_1$-$12k$ interactions.

Owing to the large magnetocrystalline anisotropy, high Curie temperature T_c and saturation magnetization M_s, barium hexaferrites [$BaFe_{12}O_{19}$, BaM] are of great interest for magnetic recording, microwave magnetic devices, and permanent magnets[1–3]. Many schemes[3–7] have been attempted in the past few decades to improve the intrinsic magnetic properties of barium hexaferrites. The typical representative is La-based substitutions[8–10]. La-substitutions, which are benefit to improve the saturation magnetization and magnetocrystalline anisotropy, however, are detrimental to enhance the Curie temperature[8–10,11]. With the requirements of wide operating temperature range of microwave devices and components, it is very important to quantitatively explore the relationship between the Curie temperature T_c and exchange integrals.

The Heisenberg model provides an opportunity to realize account for a large amount of the basic physical laws of ferrites from a phenomenological description. Especially, for a wide range of spinel ferrites[12,13], the exchange interactions have been investigated based on the molecular field theory employing the generalized gradient approximation (GGA) and local spin density approximation (LSDA) methods. So far, the work of the relationship between the Curie temperature T_c and exchange integrals for barium hexaferrites has been mainly concentrated on the undoped samples using the nonlinear fitting methods: Isalgué *et al.*[14] suggested that $12k$ sublattice of barium hexaferrites is subject to a strong exchange interaction for the sake of the link between R (R^*) and S (S^*) blocks, and Grill *et al.*[15] confirmed that Fe^{3+}_{2b}-O-Fe^{3+}_{4f2}, Fe^{3+}_{2a}-O-Fe^{3+}_{4f1}, Fe^{3+}_{4f2}-O-Fe^{3+}_{12k}, and Fe^{3+}_{4f1}-O-Fe^{3+}_{12k} triads demonstrate the comparatively strong exchange coupling. Unfortunately, the above calculations neglect the intra-sublattice interactions and strongly correlated $3d$ electrons of Fe, and then overestimate the exchange integrals and Curie temperature T_c.

In short, in terms of La-substituted barium hexaferrites, there are seldom researches that quantitatively explore the relationship between the Curie temperature T_c and exchange integrals. And the exchange integrals as a function of the effective value U_{eff} have not been also investigated completely within the framework of the density functional theory. Furthermore, the Curie temperature T_c has not been realized based on the exchange

[1]State Key Laboratory of Electronic Thin Films and Integrated Devices, University of Electronic Science and Technology of China, Chengdu 610054, China. [2]Department of Applied Physics, University of Electronic Science and Technology of China, Chengdu 610054, China. Correspondence and requests for materials should be addressed to C.W. (email: wcjuestc2005@gmail.com) or K.S. (email: ksun@uestc.edu.cn)
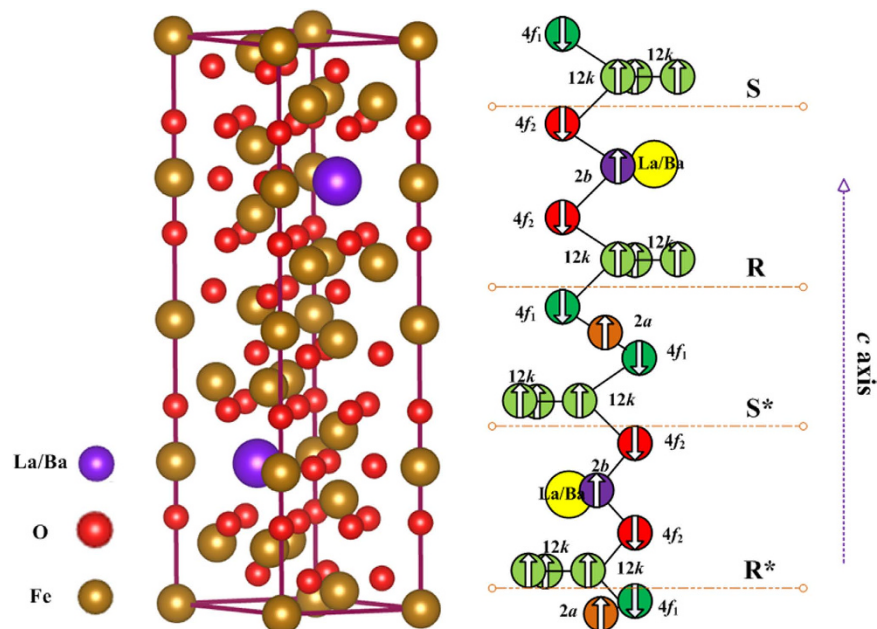
Figure 1. The unit cell and spin configurations for $Ba_{1-x}La_xFe_{12}O_{19}$: Purple, red, and gold spheres denote Ba/La, O and Fe atoms. The arrows represent the local magnetic moment at each atom site.
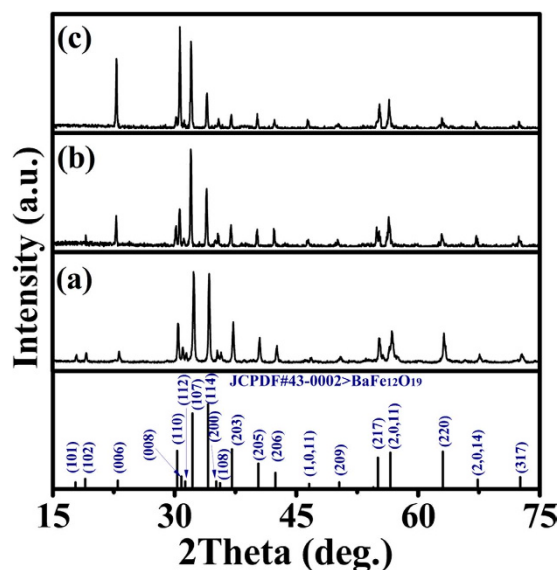

Figure 2. The X-ray diffraction patterns for $Ba_{1-x}La_xFe_{12}O_{19}$ samples. (a) $x = 0.0$, **(b)** $x = 0.5$, **(c)** $x = 1.0$. And the main (hkl) peaks from JCPDF Card No. 43–0002 for $BaFe_{12}O_{19}$ are also plotted.

integrals by the molecular field approximation (MFA) and random phase approximation (RPA) methods. So this paper would focus on solving these issues.

Results and Discussion

Crystal and Magnetic structure. The crystal structure of M-type hexaferrites could be described as SRS^*R^*, where $S = (Fe_6^{3+}O^{2-}{}_8)^{2+}$ is a spinel block with only two layers, and $R = (Ba^{2+}Fe_6^{3+}O^{2-}{}_{11})^{2-}$ is a barium containing hexagonal block with three oxygen layers: S^* and R^* are obtained from S and R blocks, respectively, by a rotation of 180° about c axis[16]. As shown in Fig. 1, 24 Fe^{3+} ions of M-type hexaferrites are distributed in five different sublattices: 3 parallel sites ($12k$, $2a$ and $2b$) and 2 antiparallel sites ($4f_1$ and $4f_2$)[17]. La-based substitutions could contribute to some Fe^{3+} transforming into Fe^{2+} at the $2a$ and $4f_2$ sites[18]. The X-ray diffraction (XRD) patterns indicated that the compounds are crystallized in a magnetoplumbite hexagonal structure (see Fig. 2). According to the relationship between the cation distribution and the magnetic moments at 0 K[19,20], the cation distribution of La-substituted barium hexaferrites is summarized in Table 1. In order to conform the results, the
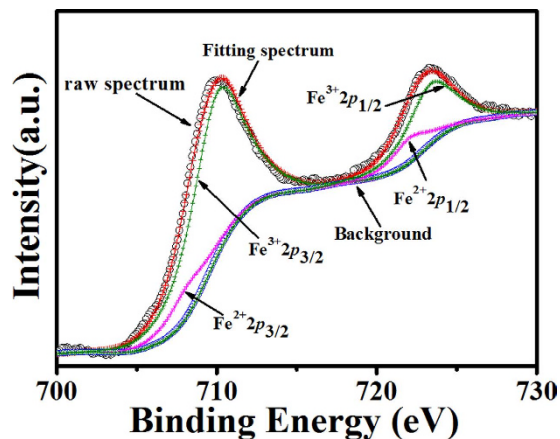
2

Figure 3. The representative XPS spectra of iron ions for $LaFe_{12}O_{19}$ sample.

Samples	σ_s (emu/g)	Cation distribution
$x=0.0$	100.50	$(Ba^{2+}Fe_2^{3+}[Fe^{3+}]O_3^{2-} \quad Fe_2^{3+}[(Fe^{3+})(Fe_6^{3+})]O_{16}^{2-})_2$ [24]
$x=0.5$	100.31	$(Ba_{0.5}^{2+}La_{0.5}^{3+}Fe_{1.762}^{3+}Fe_{0.238}^{2+}[Fe^{3+}]O_3^{2-} \quad Fe_2^{3+}[(Fe_{0.738}^{3+}Fe_{0.262}^{2+})(Fe_6^{3+})]O_{16}^{2-})_2$
$x=1.0$	100.28	$(La^{3+}Fe_{1.508}^{3+}Fe_{0.492}^{2+}[Fe^{3+}]O_3^{2-} \quad Fe_2^{3+}[(Fe_{0.492}^{3+}Fe_{0.508}^{2+})(Fe_6^{3+})]O_{16}^{2-})_2$

Table 1. The cation distribution for $Ba_{1-x}La_xFe_{12}O_{19}$ samples.

	2a		2b		4f₁		4f₂		12k	
	z_{ij}	r_{ij}	z_{ij}	r_{ij}	z_{ij}	r_{ij}	z_{ij}	r_{ij}	z_{ij}	r_{ij}
2a	6	0.589	2	0.580	6	0.346	6	0.557	6	0.305
2b	3	0.580	6	0.589	6	0.619	6	0.367	6	0.371
4f₁	2	0.346	3	0.619	3	0.363	1	0.379	6	0.350
									3	0.356
4f₂	3	0.557	3	0.367	1	0.379	1	0.277	6	0.351
12k	1	0.305	1	0.371	2	0.350	2	0.351	2	0.291
					1	0.356			2	0.298

Table 2. The number of nearest Fe neighbors and corresponding distance for five sublattices in the $BaFe_{12}O_{19}$.

photoelectron counting area of Fe^{2+} and Fe^{3+} ions is presented in Fig. 3, and the molar ratio of $Fe^{2+}/(Fe^{2+}+Fe^{3+})$ for $LaFe_{12}O_{19}$ sample is approximately 9%.

Ab initio calculation of exchange interactions. For the exchange interaction between two spins in the isotropic Heisenberg mode, the ferrimagnetic spin configurations (up or down) are considered. The exchange energy per unit cell in the complex system with N magnetic sublattices could be then written as

$$E_{ex} = \frac{1}{2}\sum_{i=1}^{N}\sum_{j\neq i=1}^{N} n_i z_{ij} J_{ij} S_i S_j \sigma_i^{(\alpha)} \sigma_j^{(\alpha)}$$

(1)

where n_i is the number of ith sublattice, z_{ij} is the number of neighboring sites in jth sublattice to ith sublattice, J_{ij} is the exchange integrals, S_i and S_j represent the spins in the ith and jth sublattices, $\sigma_i^{(\alpha)}$ and $\sigma_j^{(\alpha)}$ are equal to ± 1, and the index α is the spin arrangement of the sublattices. We denote α_0 as the ground state, and α_n ($n\neq 0$) as the relative state. The neighboring z_{ij} and corresponding distance r_{ij} for five sublattices are given in Table 2. The difference between the exchange energy of α_n and α_0 is

$$\Delta(\alpha_n - \alpha_0) = \frac{1}{2}\sum_{i=1}^{N}\sum_{j\neq i=1}^{N} n_i z_{ij} J_{ij} S_i S_j (\sigma_i^{(\alpha_n)}\sigma_j^{(\alpha_n)} - \sigma_i^{(\alpha_0)}\sigma_j^{(\alpha_0)})$$

(2)

Note that $n_i z_{ij} = n_j z_{ji}$. When the spin of a single sublattice is inverted relative to the ground state, we get

S_1	S_2	$\triangle(3.4)$	$\triangle(6.7)$	$\triangle(10.4)$
$2a$	—	0.853	0.607	0.565
$2b$	—	0.802	0.476	0.285
$4f_1$	—	3.218	1.647	0.951
$4f_2$	—	3.349	1.814	1.268
$12k$	—	3.986	1.972	1.244
$2a$	$2b$	1.649	1.082	0.853
$2a$	$4f_1$	1.882	0.861	0.762
$2a$	$4f_2$	4.201	2.420	1.831
$2a$	$12k$	5.128	2.598	1.800
$2b$	$4f_1$	3.921	2.086	1.260
$2b$	$4f_2$	1.694	0.835	0.741
$2b$	$12k$	5.707	2.918	1.795
$4f_1$	$4f_2$	6.738	3.545	2.252
$4f_1$	$12k$	2.548	0.758	0.341
$4f_2$	$12k$	2.718	0.842	0.673
$2f_1$	—	1.556	0.809	0.470
$2f_2$	—	1.645	0.891	0.633
$4k$	—	0.758	0.453	0.267
$8k$	—	2.013	0.963	0.781

Table 3. The energy difference $\triangle(U_{\text{eff}})$ in eV between the ground state and excited state.

$$\Delta(\alpha_i - \alpha_0) = -2S_i n_i \sum_{j \neq i} z_{ij} J_{ij} S_j \sigma_i^{(\alpha_0)} \sigma_j^{(\alpha_0)} \tag{3}$$

When the spins of two sublattices inverted relative to the ground state are considered, we then obtain.

$$\Delta(\alpha_{ij} - \alpha_0) = \Delta(\alpha_i - \alpha_0) + \Delta(\alpha_j - \alpha_0) + 4n_i z_{ij} J_{ij} S_i S_j \sigma_i^{(\alpha_0)} \sigma_j^{(\alpha_0)} \tag{4}$$

Thereby the exchange integral could be given by

$$J_{ij} = \frac{\Delta(\alpha_{ij} - \alpha_0) - \Delta(\alpha_i - \alpha_0) - \Delta(\alpha_j - \alpha_0)}{4n_i z_{ij} S_i S_j \sigma_i^{(0)} \sigma_j^{(0)}} \tag{5}$$

As mentioned above, the Fe^{3+} and Fe^{2+} ions in the five sublattices are anti-ferromagnetically coupled with each other. The orbit angular momentum is frozen and hence the magnetism of the Fe^{3+} and Fe^{2+} ions mainly results from the spin angular momentum $S = 2.5$ and $S = 2.0$, respectively[20]. For the mixed valence Ba/La hexaferrites, the spin angular momentum S_i in the ith sublattice could be assumed to be.

$$S_i = \frac{t_1 S_{Fe^{3+}} + t_2 S_{Fe^{2+}}}{t_1 + t_2} \tag{6}$$

where t_1 and t_2 are the Fe^{3+} and Fe^{2+} numbers in the ith sublattice, respectively. Since the exchange interactions between two magnetic ions decrease with the increase of the corresponding distance, the distance more than 4 Å could be neglected[21]. As shown in Table 2, the distance of neighboring $4f_1$, $4f_2$, and $12k$ sublattices is smaller than 4 Å, and in fact these sublattices have also the nearest Fe neighbors in the same sublattices. Ten inter-sublattice interactions ($2a$-$2b$, $2a$-$4f_1$, $2a$-$4f_2$, $2a$-$12k$, $2b$-$4f_1$, $2b$-$4f_2$, $2b$-$12k$, $4f_1$-$4f_2$, $4f_1$-$12k$, and $4f_2$-$12k$) and three intra-sublattice interactions ($4f_1$-$4f_1$, $4f_2$-$4f_2$, and $12k$-$12k$) were thus considered. For intra-sublattice interaction calculations, in order to preserve the highest symmetry, one divided the $4f_1$, $4f_2$, and $12k$ sublattices into ($2f_1$, $2f_1$), ($2f_2$, $2f_2$), and ($4k$, $8k$), respectively. The representative calculations ($x = 0.5$) of energy difference per unit cell for each relative state are given in Table 3. According to the Eq. (5), thirteen exchange integrals as a function of U_{eff} (see Fig. 4) could be obtained. The $2a$-$2b$ and $2a$-$4f_2$ interactions are very small with $|J_{2a\text{-}2b}|$ and $|J_{2a\text{-}4f2}| < 0.05$, which is ascribed to the Fe_{2a}-O-Fe_{2b}, and Fe_{2a}-O-Fe_{4f2} angles approach 90°[14]. The different ionic radii of La^{3+} (1.22 Å), and Ba^{2+} (1.47 Å)[11] causes some changes in exchange interactions of Ba/La hexaferrites: The $2a$-$4f_1$, $2a$-$12k$, $2b$-$4f_1$, and $2b$-$12k$ interactions increase, and whilst the $4f_1$-$4f_2$, $4f_1$-$12k$, $4f_2$-$12k$, $2f_1$-$2f_1$, $2f_2$-$2f_2$, and $4k$-$8k$ interactions decrease with the increase of La concentrations. It is emphasized, however, $2b$-$4f_2$ interaction has a slight change (about 0.1 eV). This is associated with the strong effects of barium or lanthanum ions on the nearest neighboring iron ions ($2b$ and $4f_2$ sublattices)[22].

Calculations of Curie temperature.

In the following one calculated the Curie temperature T_c employing the Heisenberg Hamiltonian. The common calculations of Curie temperature T_c derived from the Heisenberg model contain the mean-filed approximation (MFA) and random-phase approximation (RPA) methods[23].

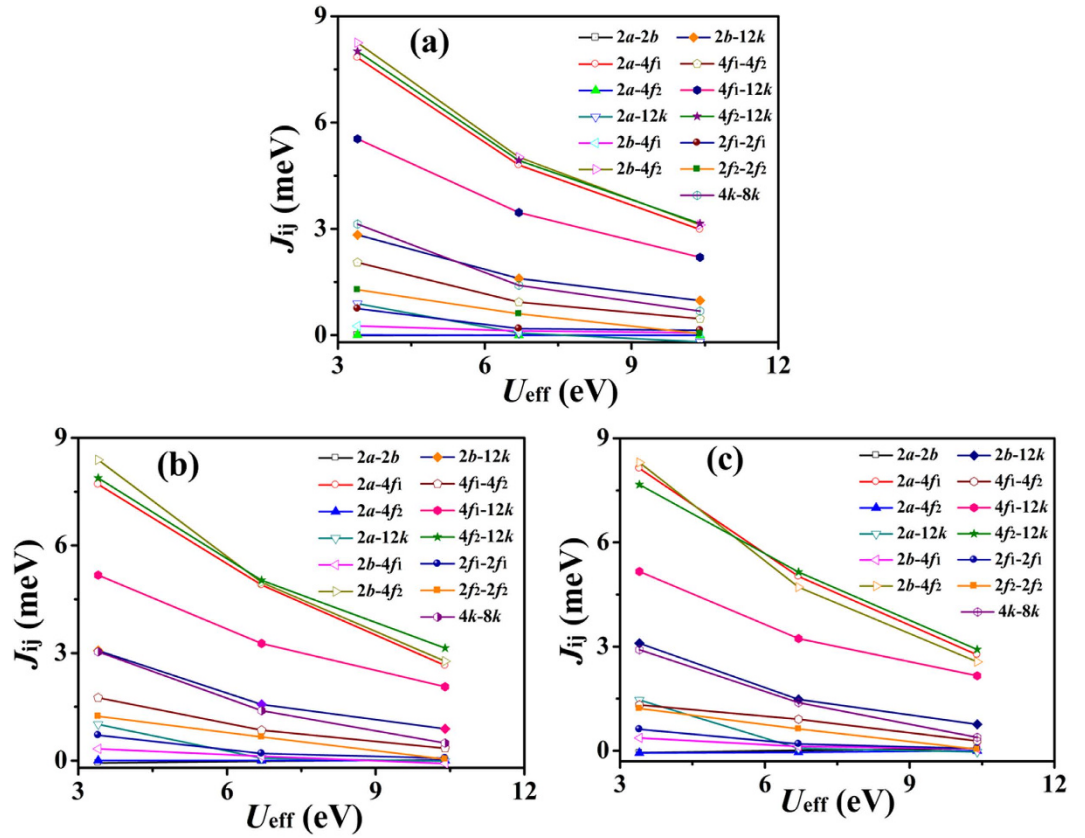The mean-field approximation is based on the notion of single-spin excitations, and the Hamiltonian is[24]

Figure 4. The exchange integrals as a function of U_{eff} for Ba$_{1-x}$La$_x$Fe$_{12}$O$_{19}$ samples. (**a**) $x = 0.0$, (**b**) $x = 0.5$, (**c**) $x = 1.0$.

$$\hat{h}_i = -\vec{\mu}_i \cdot \vec{H}_i = -g\mu_B \vec{S}_i \cdot \vec{H}_i \tag{7}$$

where g and μ_B are the Lande factor and Bohr magneton, respectively. The molecular field $\vec{H}_i$ could be thus defined as

$$\vec{H}_i = -\frac{1}{g\mu_B}\sum_j J_{ij} <\vec{S}_j> \tag{8}$$

with

$$<S_{iz}> = S_i B_{S_i}(x_i), \; x_i = \frac{g\mu_B H_i}{k_B T} \tag{9}$$

where $B_{S_i}(x_i)$ is the Brillouin function, k_B is the Boltzmann constant, and T is the temperature in K. When T is very high, such as $k_B T \gg \mu_B H_i$, the $B_{S_i}(x_i)$ and $<S_{iz}>$ are rewritten as

$$B_s(x) = \frac{(S+1)x_i}{3}, \;\; <S_{iz}> = \frac{S_i(S_i+1)g\mu_B H_i}{3k_B T} \tag{10}$$

Introducing the exchange integral J_{ij}, we get

$$<S_{iz}> = -\frac{S_i(S_i+1)}{3k_B T}\sum_j J_{ij} <S_{jz}> \tag{11}$$

i.e.,

$$T<S_{jz}> + \frac{S_i(S_i+1)}{3k_B}\sum_j J_{ij} <S_{jz}> = 0 \tag{12}$$

which has nonzero solution only if the determinant

U_{eff} (eV)	$x = 0.0$			$x = 0.5$			$x = 1.0$		
	3.4	6.7	10.4	3.4	6.7	10.4	3.4	6.7	10.4
E.V. (K)	723	723	723	705	705	705	695	695	695
MFA (K)	1514	980	629	1450	951	581	1419	928	579
RPA (K)	1009	653	419	967	634	387	946	619	386

Table 4. The experimental and calculating Curie temperature as a function of U_{eff} for $Ba_{1-x}La_xFe_{12}O_{19}$ samples.

$$\begin{vmatrix} a_{11} - T & \cdots & \cdots & a_{1n} \\ \cdots & & & \cdots \\ a_{n1} & a_{n2} & \cdots & a_{nn} - T \end{vmatrix} = 0, \quad a_{ij} = -\frac{S_i(S_i + 1)}{3k_B}J_{ij},$$ (13)

In fifth order systems, there are five solutions in Eq. (13). The highest positive T is the desired Curie temperature T_c.

In the random-phase approximation, it is assumed that the thermal disordering is achieved by the excitation of independent spin waves[25]. The equation of motion for the Green function (analogously to Callen)[26] is given that

$$\frac{\partial}{\partial \tau}G_{ij}^{AB}(\tau) = -\frac{i}{\hbar}\delta(\tau)\langle[\hat{s}_{i,A}^+, \exp(a\hat{s}_{j,B}^z)\hat{s}_{j,B}^-]\rangle - \frac{1}{\hbar^2}\Phi(\tau) \times \langle[[\hat{s}_{i,A}^+(\tau), \hat{H}], \exp(a\hat{s}_{j,B}^z)\hat{s}_{j,B}^-]\rangle$$ (14)

where α, $\delta(\tau)$, $\Phi(\tau)$ and $\hat{s}_{i,A}^z$ are an auxiliary, unit-impulse function, unit-step function, and spin operators operating in the unit cell i at the basis site. Here $[\hat{X}, \hat{Y}] = \hat{X}\hat{Y} - \hat{Y}\hat{X}$ is a commutator, $\hat{s}_{i,A}^\pm = \hat{s}_{i,A}^x \pm i\hat{s}_{i,A}^y$, and the mean value $\langle\hat{A}\rangle = \text{Tr}[\rho\hat{A}] = \text{Tr}[\exp(-\beta\hat{H})\hat{A}]/\text{Tr}[\exp(-\beta\hat{H})]$ with $\hat{H}$ being the Heisenberg Hamiltonian and $\beta = 1/(k_BT)$. According to Tyablikov $\langle[\hat{s}_{i,A}^+\hat{s}_{j,B}^z, \hat{X}(-\tau)]\rangle \approx \langle\hat{s}_{j,B}^z\rangle\langle[\hat{s}_{i,A}^+, \hat{X}(-\tau)]\rangle$[27], the double commutator could be simplified by applying the RPA decoupling. For convenience, the matrix $N(q)$ could be defined as

$$N_{AB}(q) = \delta_{AB}\sum_C J_{AC}(0)\langle\hat{s}_C^z\rangle - \langle\hat{s}_A^z\rangle J_{AB}(q)$$ (15)

After performing time and lattice Fourier transformations, the Green's function could be expressed by the following form

$$G_{AB}(\omega; q) = \frac{1}{2\pi}\langle[\hat{s}_{i,A}^+, \exp(a\hat{s}_{j,A}^z)\hat{s}_{j,A}^-]\rangle\{[\hbar\omega I - N(q)]^{-1}\}_{AB}$$ (16)

where I is unity matrix. Based on the solutions of Green's function, as described in Ref. 28, the self-consistent equation for the mean values could be written as

$$\langle\hat{s}_A^z\rangle = \frac{2S_A(S_A + 1)}{3k_BT_c}\left(\frac{1}{\Omega}\int dq[N^{-1}(q)]_{AA}\right)^{-1}$$ (17)

where T_c is the Curie temperature, k_B is the Boltzmann constant, and S_A is the spin quantum numbers. By the iterative methods to solve this self-consistent set of $<\hat{s}_A^z>$, the Curie temperature T_c could be then obtained.

Table 4 shows the experimental and calculating values of Curie temperature. It is concluded that the experimental Curie temperature is reproduced by calculations for the effective value $U_{eff} \approx 6.7$ eV, and the MFA and RPA estimations provide an upper and lower bound of the Curie temperature. In the case of La-substituted barium hexaferrites, the T_c determined by the RPA is in good agreement with the experimental T_c. This could be explicated: the fluctuations of spin wave in MFA (i.e., fluctuations in the magnitudes of the atomic moments) are generally neglected, and hence the arithmetic average takes all the magnon values with the equal weight. While in RPA, this is the harmonic average, and the weight decreases with the increasing spin-wave energy[25,28].

Conclusions

The composition of $Ba_{1-x}La_xFe_{12}O_{19}$ ($x = 0.0$, 0.5 and 1.0) were prepared by a conventional ceramic method. Thirteen exchange interactions were calculated by the DFT and GGA + U. With the increase of La contents, the $2a$-$4f_1$, $2a$-$12k$, $2b$-$4f_1$, and $2b$-$12k$ interactions increase, the $4f_1$-$4f_2$, $4f_1$-$12k$, $4f_2$-$12k$, $2f_1$-$2f_1$, $2f_2$-$2f_2$, and $4k$-$8k$ interactions decrease, while the $2b$-$4f_2$ interaction has a slight change. The Curie temperature was then calculated using the MFA, and RPA estimations. The RPA is more coincident with the experiments for the effective value $U_{eff} \approx 6.7$ eV.

Methods

Experimental procedures. The compositions of $Ba_{1-x}La_xFe_{12}O_{19}$ ($x = 0.0$, 0.5 and 1.0) were fabricated by a conventional ceramic method. The analytical-grade raw materials, $BaCO_3$, La_2O_3, and Fe_2O_3 were weighed in stoichiometric proportion and mixed homogeneously in zirconia ball mills for 12 h. The slurries, after being dried,

were calcined at 800 °C for 2 h and then second-milled with 3.0 wt% Bi_2O_3 for 8 h. After being further dried at 90 °C, the powders were granulated, pressed and sintered at 1050 °C for 2 h in air. Essential for preventing decomposition into Fe_2O_3 and $LaFeO_3/BaFe_2O_4$ is rapid cooling. The X-ray diffraction (XRD) patterns were identified on Bruker D8 Advance X-ray diffractometer with Cu-Kα radiation. The binding energy of iron ions was acquired by X-ray photoelectron spectroscopy (XPS) XSAM800. The hysteresis loops of the samples at 1.8 K (approaching 0K) were measured by Quantum Design SQUID VSM under the applied static magnetic fields up to 6T. The experimental values (E.V.) of Curie temperature for La-substituted barium hexaferrites were measured by the Thermal Gravimetric Analyzer (TGA) under N_2 atmosphere using a TA-Q50 series analyzer system.

Computational details.   The total energies and forces were calculated using the density-functional theory (DFT) with the Generalized Gradient Approximation (GGA) as parameterized by the Perdew-Burke-Ernzerhof (PBE) in VASP[29,30]. In structure optimization, we adopted the Conjugate Gradient (CG) method to optimize the lattice parameters and the position of ions until the force on each ion was less than 0.03 eV/Å. The plane-wave cutoff energy and convergence criteria were 500 eV and 10^{-7} eV, respectively. The reciprocal space was sampled with an $11 \times 11 \times 1$ Monkhorst-Pack mesh[31]. All the calculations were spin polarized according to the Gorter's ferrimagnetic ordering of the magnetic moments[32]. For improved description of $3d$ electrons in iron ions, the generalized gradient approximation with Coulomb and exchange interaction effects (GGA+U) were employed, where an on-site potential is added to introduce intra-atomic interactions between the strongly correlated electrons[33]. We employed an effective value (U_{eff}) equal to the difference between the Hubbard parameter U and the exchange parameter J[34]. To study how the results depend on U_{eff}, three values (3.4, 6.7, and 10.4 eV) on Fe atoms were adopted on the basis of many rigorous calculations of barium hexaferrites[31,35,36].

References

1. Shuai, M. *et al.* Spontaneous liquid crystal and ferromagnetic ordering of colloidal magnetic nanoplates. *Nat. Commun.* **7,** 10394, 10.1038/ncomms10394 (2016).
2. Liu, C. *et al.* Multi-susceptibile single-phased ceramics with both considerable magnetic and dielectric properties by selectively doping. *Sci. Rep.* **5,** 9498, 10.1038/srep09498 (2015).
3. Shen, S. P. *et al.* Magnetic-ion-induced displacive electric polarization in FeO_5 bipyramidal units of $(Ba,Sr)Fe_{12}O_{19}$ hexaferrites. *Phys. Rev. B* **90,** 180404 (2014).
4. Vinnik, D. A. *et al.* Growth, structural and magnetic characterization of Al-substituted barium hexaferrite single crystals. *J. Alloys Compd.* **615,** 1043–1046 (2014).
5. Katlakunta, S. *et al.* Improved magnetic properties of Cr^{3+} doped $SrFe_{12}O_{19}$ synthesized via microwave hydrothermal route. *Mater. Res. Bull.* **63,** 58–66 (2015).
6. Sharma, M., Kashyap, S. C. & Gupta, H. C. Effect of Mg–Zr substitution and microwave processing on magnetic properties of barium hexaferrite. *Physica B* **448,** 24–28 (2014).
7. Alam, R. S., Moradi, M., Nikmanesh, H., Ventura, J. & Rostami, M. Magnetic and microwave absorption properties of $BaMg_{x/2}Mn_{x/2}Co_xTi_{2x}Fe_{12-4x}O_{19}$ hexaferrite nanoparticles. *J. Magn. Magn. Mater.* **402,** 20–27 (2016).
8. Singh, V. P. *et al.* Structural, magnetic and Mössbauer study of $BaLa_xFe_{12-x}O_{19}$ nanohexaferrites synthesized via sol–gel auto-combustion technique. *Ceram. Int.* **42,** 5011–5017 (2016).
9. Thakur, A., Barman, P. B. & Singh, R. R. Effects of La^{3+}–Nd^{3+} ions and pre-calcination on the growth of hexaferrite nanoparticles prepared by gel to crystallization technique: Non-isothermal crystallization kinetics analysis. *Mater. Chem. Phys.* **156,** 29–37 (2015).
10. Piper, M. W., Kools, F. & Morel, A. NMR characterization of Co sites in La^+Co-doped Sr hexaferrites with enhanced magnetic anisotropy. *Phys. Rev. B* **65,** 184402 (2002).
11. Liu, X. *et al.* Influences of La^{3+} substitution on the structure and magnetic properties of M-type strontium ferrites. *J. Magn. Magn. Mater.* **238,** 207–214 (2002).
12. Xu, Z. & Carmine, V. Calculation of exchange integrals and electronic structure for manganese ferrite. *Phys. Rev. B* **66,** 184420 (2002).
13. Perron, H. *et al.* Structural investigation and electronic properties of the nickel ferrite $NiFe_2O_4$: a periodic density functional theory approach. *J. Phys.: Condens. Matter.* **19,** 346219 (2007).
14. Isalgué, A., Labarta, A., Tejada, J. & Obradors, X. Exchange interactions in $BaFe_{12}O_{19}$. *Appl. Phys. A* **39,** 221–225 (1986).
15. Grill, A. & Haberey, F. Effect of diamagnetic substitutions in $BaFe_{12}O_{19}$ on the magnetic properties. *Appl. Phys.* **3,** 131–134 (1974).
16. Din, M. F. *et al.* Influence of Cd substitution on structural, electrical and magnetic properties of M-type barium hexaferrites co-precipitated nanomaterials. *J. Alloys Compd.* **584,** 646–651 (2013).
17. Dixit, V. *et al.* Site occupancy and magnetic properties of Al-substituted M-type strontium hexaferrite. *J. Appl. Phys.* **118,** 203908 (2015).
18. Van Diepen, A. M. & Lotgering, F. K. Mössbauer effect in $LaFe_{12}O_{19}$. *J. Phys. Chem. Solids* **35,** 1641–1643 (1974).
19. Anderson, P. W. Antiferromagnetism. Theory of superexchange interaction. *Phys. Rev.* **79,** 350–356 (1950).
20. Wu, C. *et al.* Brillouin function characteristics for La-Co substituted barium hexaferrites. *J. Appl. Phys.* **118,** 103907 (2015).
21. Néel, L. Magnetism and local molecular field. *Science* **174,** 985–992 (1971).
22. Pullar, R. C. Hexagonal ferrites: a review of the synthesis, properties and applications of hexaferrite ceramics. *Prog. Mater. Sci.* **57,** 1191–1334 (2012).
23. Sandratskii, L. M. & Bruno, P. Exchange interactions and curie temperature in (Ga, Mn)As. *Phys. Rev. B* **66,** 134435 (2002).
24. Pajda, M., Kudrnovský, J., Turek, I., Drchal, V. & Bruno, P. Ab initio calculations of exchange interactions, spin-wave stiffness constants, and Curie temperatures of Fe, Co, and Ni. *Phys. Rev. B* **64,** 174402 (2001).
25. Morán, S., Ederer, C. & Fähnle, M. Ab initio electron theory for magnetism in Fe: Pressure dependence of spin-wave energies, exchange parameters, and Curie temperature. *Phys. Rev. B* **67,** 012407 (2003).
26. Callen, H. B. Green function theory of ferromagnetism. *Phys. Rev.* **130,** 890–898 (1963).
27. Tyablikov, S. V. Lagging and Anticipating Green Functions in the Theory of Ferromagnetism. *Ukr. Mat. Zhur* **11,** 287–294 (1959).
28. Rusz, J., Turek, I. & Diviš, M. Random-phase approximation for critical temperatures of collinear magnets with multiple sublattices: GdX compounds (X = Mg, Rh, Ni, Pd). *Phys. Rev. B* **71,** 174408 (2005).
29. Perdew, J. P., Burke, K. & Ernzerhof, M. Generalized gradient approximation made simple. *Phys. Rev. Lett.* **77,** 3865–3868 (1996).
30. Kresse, G. & Joubert, D. From ultrasoft pseudopotentials to the projector augmented-wave method. *Phys. Rev. B* **59,** 1758–1775 (1999).
31. Fang, M., Shao, B., Lu, Y. & Zuo, X. Ab initio study on magnetic anisotropy change of $SrCo_xTi_xFe_{12-2x}O_{19}$. *J. Appl. Phys.* **115,** 17D908 (2014).

32. Gorter, E. W. Chemistry and magnetic properties of some ferrimagnetic oxides like those occurring in nature. *Adv. Phys.* **6,** 336–361 (1957).
33. Dudarev, S. L., Botton, G. A., Savrasov, S. Y., Humphreys, C. J. & Sutton, A. P. Electron-energy-loss spectra and the structural stability of nickel oxide: An LSDA+ U study. *Phys. Rev. B* **57,** 1505–1509 (1998).
34. Park, J. *et al.* Maximum energy product at elevated temperatures for hexagonal strontium ferrite ($SrFe_{12}O_{19}$) magnet. *J. Magn. Magn. Mater.* **355,** 1–6 (2014).
35. Knížek, K. *et al.* Structural phase transition and magnetic anisotropy of La-substituted M-type Sr hexaferrite. *Phys. Rev. B* **73,** 144408 (2006).
36. Liyanage, L. S. I. *et al.* Theory of magnetic enhancement in strontium hexaferrite through Zn–Sn pair substitution. *J. Magn. Magn. Mater.* **348,** 75–81 (2013).

Author Contributions

C.W. designed the work progress and wrote the manuscript; R.G. and H.L. performed the measurements; C.W., Z.Y., K.S., R.G., J.N., X.J. and Z.L. analyzed the results and conceived the central idea. All authors reviewed the manuscript.

Additional Information